Journal of Zhejiang University-SCIENCE A (Applied Physics & Engineering)
ISSN 1673-565X (Print); ISSN 1862-1775 (Online)
www.jzus.zju.edu.cn; www.springerlink.com
E-mail: jzus@zju.edu.cn

Interaction between patch loading, bending moment, and shear stress in steel girders

Emanuele MAIORANA[1], Cyrille Denis TETOUGUENI[2], Paolo ZAMPIERI[†‡2], Carlo PELLEGRINO[2]

[1]*Collegio dei Tecnici dell'Acciaio (CTA), Viale dei Mille 19, 20129 Milano, Italy*

[2]*Department of Civil, Environmental and Architectural Engineering, University of Padova, Via Marzolo 9, 35131 Padova, Italy*

[†]E-mail: paolozampieri@dicea.unipd.it

Received Jan. 23, 2019; Revision accepted Apr. 26, 2019; Crosschecked May 9, 2019

Abstract: In bridge erection, a steel girder undergoing in-plane loading is commonly subjected to the interaction of several forces. Many previous studies have highlighted the effects of single in-plane loads on plate buckling but only a few works concentrated on the combined effects. For this reason, the stability of steel plates subjected to the combined action of patch loading, bending moment, and shear stress was studied through parametric analysis in this work. In particular, the effect of patch loading length combined with bending and shear stress was investigated. Other parameters like patch loading magnitude, panel aspect ratio, and plate slenderness have also been considered to characterize the plate stability. Through an intensive finite element method (FEM) analysis, new design equations have been defined to describe the influence of plate and load parameters on critical buckling loads of plates subjected to combined loads, with regard to plates subjected to patch loading. A comparison with the FEM results offers good accuracy, with a maximum deviation equal to 5%. To validate the analytical equations, a practical example is given.

Key words: Elastic stability; Patch loading; Finite element method (FEM) analysis; Steel bridges erection
https://doi.org/10.1631/jzus.A1900024 **CLC number:** TU39

1 Introduction

Different technologies are used for bridge erection around the world, among which, the incremental launching method appears to be preferred according to the statistics presented by many researchers (Kövesdi et al., 2014; Graciano and Zapata-Medina, 2015; Kövesdi and Dunai, 2016; Tetougueni et al., 2019). Although it is not considered the most economical technique, the incremental launching method has become unavoidable in bridge construction over a wide range of challenging sites that feature limited or restricted access such as valleys, deep water crossings, steep slope conditions, and protected species beneath the bridge. During the launching process, slender girders may overpass at least one time on bearings where a concentrated force from the support reaction may arise. In addition, as the beam is pulled from one support to another and considering the self-weight of both of the girder and equipment as well as other construction loads, a large bending moment and shear force can also arise. If special attention is not taken with the steel girders, the instability of the slender web will occur leading to the loss of the section in the construction phase.

The current EN1993-1-5 standard (CEN, 2006) provides verification methods for a steel plate subjected to patch loading, bending, shear, and buckling. In addition, for a steel plate subjected to the following in-plane loads, such as bending–patch loading (*M*-*F*), bending–shear buckling (*M*-*V*), and shear buckling–patch loading (*V*-*F*) interactions, the associated interaction equations are found within the EN1993-1-5

‡ Corresponding author
ORCID: Paolo ZAMPIERI, https://orcid.org/0000-0002-4556-5043

standard (CEN, 2006) for design in such situations. In the meantime, the lack of a straightforward *M*-*V*-*F* interaction equation in the design standard has forced many researchers to address this issue. In 2010, during his PhD thesis, Braun (2010) developed 3D interaction curves to design a steel plate under combined in-plane loadings. The 3D domain was built from the database of the numerical results of both *M*-*F* and *V*-*F* interactions. Later, Graciano and Ayestarán (2013) and Kövesdi et al. (2014) provided more general and accurate 3D interaction curves obtained from merging the individual *M*-*F*, *V*-*F*, and *M*-*F* interaction curves. The two studies combined offer a wide range of applicability since each research work was based on the analysis of different geometrical parameter ranges (Kövesdi et al., 2014). The interest shown for the design of the steel plate's stability in the case of combined in-plane loading is less than that observed for the 3D interaction design resistance. In this regard, Tong et al. (2016) proposed 3D non-dimensional interactive surfaces to describe the stability of a steel plate subjected to combined patch loading, bending, and shear force. The interaction equation derived covers a wide range of variability in the steel girder geometry.

From parts of the previous studies, it appears that both the stability and ultimate capacity of a steel plate under different loading conditions have been intensively investigated but till now, only a few studies have directed their research toward a steel plate subjected to combined *M*-*F*-*V* loading. In addition, all the existing studies' outcomes solved the problem through the 3D interaction domain while most of the time, designers and practitioners are looking for straightforward analytical expressions that are useful in the predesign stage before moving ahead into the design phase.

In the present research, intensive numerical analyses were performed to derive a unique equation to determine the critical buckling load multiplier of a steel plate under combined *M*-*V*-*F* loading. In addition, a large portion of the authors' previous work (Maiorana et al., 2008) developed an innovative equation to determine the critical patch loading for a steel plate under combined in-plane loading. A detailed description of the research aim is found in the next section at the end of the literature review. The study was completed systematically following the research strategy listed below. In particular, the following points will be discussed.

1. Literature overview of work on steel plate behavior under combined in-plane loading, both singular and combined.

2. Development of numerical models based on Quad 4 shell elements taking into account different aspects related to the steel plate's geometry and loading conditions and validation of the numerical model based on previous experimental, analytical, and finite element method (FEM) analysis results.

3. Parametric numerical analysis to study the structural behavior of a steel plate subjected to combined in-plane loadings such as buckling shape and critical buckling load factor; different geometrical and loading parameters will be considered.

4. Development of a design equation to determine the critical buckling load multiplier based on FEM results; validation of the proposed equations through a comparison of the analytical equation proposed and the FEM results.

5. Application of the proposed formula in a design example to show the applicability of the formula in a real world situation.

The research results showed that additional bending and shear loadings may considerably reduce the critical patch loading resistance up to 50%. On the other hand, high accuracy was obtained comparing both FEM and analytical results with a discrepancy lower than 5%. Finally, through a practical example, the current research results showed their reliability in application to a real world design.

2 Literature review

The instability of a steel plate subjected to various loading conditions has been widely studied either experimentally or numerically. The topic became a definitive research interest after the collapse of some bridges due to the loss of stability in the 1950s with the presentation of the first results on a related topic. For the most part, the results were based on experimental campaigns and theoretical investigations. Several researchers such as Zetlin (1955), Basler (1961), Rockey and Bagchi (1970), and Khan and Walker (1972) derived the critical buckling coefficient of both clamped and simply supported steel

plates subjected to partial edge loading. Recently, there have been substantial research works that have been carried out with the aim of either studying new aspects or providing further details and explanations of the pioneering research.

Graciano and Lagerqvist (2003) studied the stability of a steel plate under compressive loads. They considered the rotational restraint of the flange in the definition of the critical buckling coefficient of a simply supported plate. Ren and Tong (2005) focused their research on the restraining conditions of the plate girder web. They proposed a buckling coefficient in terms of patch loading for both simply supported and clamped rectangular plates (Eqs. (1) and (2)).

$$k_{\mathrm{crs}}=2.05+12\Big/\left(a/h_{\mathrm{w}}\right)^2+s_{\mathrm{s}}^2\left[0.5+2.0\Big/\left(a/h_{\mathrm{w}}\right)^2\right], \quad (1)$$

$$k_{\mathrm{crf}}=\left(1+0.65s_{\mathrm{s}}^2\right)\left[6.3-0.5+2.0\Big/\left(a/h_{\mathrm{w}}\right)^2\right], \quad (2)$$

where k_{crs} is the elastic buckling coefficient of simply supported plates under patch loading, k_{crf} is the elastic buckling coefficient of clamped plates under patch loading, s_{s} is the patch loading length, a is the length of the steel plate (length between successive vertical stiffeners), and h_{w} is the height of the web panel.

Other expressions to determine the critical buckling coefficient were proposed (Duchene and Maquoi, 1994; Maiorana et al., 2008). Porter and Rockey (1975) studied the critical condition of plate girders. Through extensive numerical analysis, Alinia (2005) investigated the critical buckling of a stiffened plate under shear while Maiorana et al. (2011) studied the optimal position of a longitudinal stiffener for plates subjected to bending. Graciano and Mendes (2014) used a factorial design to study the influence of geometrical parameters on the critical buckling coefficient of a stiffened steel girder subjected to patch loading. The proposed method is useful to predict output variables from input data through a mathematical model. They found that the relative position of the stiffener, its flexural rigidity, and the patch loading length are the most influential parameters for plate buckling.

In regards to studies on steel plate stability under combined in-plane loading, an analytical formula was proposed to estimate the critical buckling coefficient of a steel plate under patch loading and bending moment (Maiorana et al., 2008). The influence of the longitudinal stiffener on the interaction curves describing the plate stability subjected to bending–shear interaction has also been studied (Alinia and Moosavi, 2009). Within the same scope, Quang-Viet et al. (2019) carefully studied the optimum position of a multi-stiffened plate under combined bending and shear forces through the gradient-based interior point optimization algorithm. The results showed that the presence of two stiffeners on a steel plate would increase the critical buckling coefficient up to 180% and may lead to the optimization of the plate thickness to approximatively 62%.

Shahabian and Roberts (1999) investigated the buckling of rectangular plates subjected to a combination of in-plane patch loading, compression, bending, and shear stress. They proposed different equations according to a case study that had a wide range of validity (Eqs. (3)–(5)).

$$\left(\frac{k_{\mathrm{bp}}}{k_{\mathrm{b}}}\right)^{\alpha_1}+\left(\frac{k_{\mathrm{pb}}}{k_{\mathrm{p}}}\right)^{\alpha_1}=1, \quad (3)$$

$$\left(\frac{k_{\mathrm{sp}}}{k_{\mathrm{s}}}\right)^{\alpha_2}+\left(\frac{k_{\mathrm{ps}}}{k_{\mathrm{p}}}\right)^{\alpha_2}=1, \quad (4)$$

$$\left(\frac{k_{\mathrm{sb}}}{k_{\mathrm{s}}}\right)^{\alpha_3}+\left(\frac{k_{\mathrm{bs}}}{k_{\mathrm{b}}}\right)^{\alpha_3}=1, \quad (5)$$

where k_{bp} is the buckling coefficient of steel plates under a combined bending and patch loading; k_{pb} is the buckling coefficient of steel plates under a combined patch loading and bending; k_{sp} is the buckling coefficient of steel plates under a combined shear and patch loading; k_{ps} is the buckling coefficient of steel plates under a combined patch loading and shear; k_{bs} is the buckling coefficient of steel plates under a combined bending and shear; k_{sb} is the buckling coefficient of steel plates under a combined shear and bending; k_{b}, k_{p}, and k_{s} are the buckling coefficients of steel plates under bending, patch loading, and shear, respectively; α_1, α_2, and α_3 are coefficients depending on loading conditions.

Recently, through extensive FEM analysis, 3D non-dimensional interactive surfaces have been proposed to describe the stability of a steel plate subjected to combined patch loading, bending, and shear

force (Tong et al., 2016). In the study, it is also provided a single equation to define the 3D interaction curve (Eq. (6)). Further information regarding the parameters involved in this equation is found within the paper.

$$\chi\left(\frac{\sigma_{\mathrm{b}}}{\sigma_{\mathrm{bcr0}}}\right)^{\beta}+\left(\frac{\tau}{\tau_{\mathrm{bcr0}}}\right)^{2}+\left(\frac{\sigma_{\mathrm{c}}}{\sigma_{\mathrm{cr0}}}\right)^{\beta_{\mathrm{c\tau}}}=1, \tag{6}$$

where σ_{b}, τ, and σ_{c} are the applied bending, shear, and compression stress; σ_{bcr0}, τ_{bcr0}, and σ_{cr0} are the Eulerian critical stresses for pure bending, shear, and compression stresses, respectively; χ, β, and $\beta_{\mathrm{c\tau}}$ are coefficients taking into account the interaction between stress.

Other significant studies on the ultimate resistance of a steel plate under various in-plane loadings have been done. The latest research on plated structures under *M-F* interaction behavior can be found in (Tetougueni et al., 2019). Jager et al. (2017) performed an intensive numerical analysis to investigate the *M-V* interaction behavior of longitudinally unstiffened I-girders with a slender web. They proposed a refined *M-V* interaction equation changing the index *k* from 1.0 to a higher value that better fits the numerical simulations (Eq. (7)).

$$\frac{M}{M_{\mathrm{el,eff,R}}}+\left(1-\frac{M_{\mathrm{f,R}}}{M_{\mathrm{el,eff,R}}}\right)+\left(\frac{2V}{V_{\mathrm{bw,R}}}-1\right)^{2}\le 1, \tag{7}$$

where $M_{\mathrm{f,R}}$ is the plastic moment of resistance of the section consisting of the effective area of the flanges; $M_{\mathrm{el,eff,R}}$ is the bending moment resistance depending on the cross-section class; $V_{\mathrm{bw,R}}$ is the shear buckling resistance of the web panel alone; M and V are the values of the applied bending moment and shear force, respectively.

The investigation of the ultimate load behavior of longitudinally stiffened girder webs under patch loading can be found in (Graciano and Edlund, 2003). The authors discovered that the influence of stiffener's relative flexural rigidity is less important for ultimate strength analysis due to loss of the stiffener's rigidity but it plays an important role in increasing the critical elastic buckling load of a plate girder under patch loading. Braun (2010) developed a 3D interaction formula to describe the interaction behavior of a steel plate subjected to combined patch loading, bending, and shear stress (Eq. (8)).

$$\left(\frac{P}{P_{\mathrm{R}}}\right)+\left(\frac{M}{M_{\mathrm{R}}}\right)^{3.6}+\left(\frac{V}{V_{\mathrm{R}}}\right)^{1.6}\le 1, \tag{8}$$

where the notations involved are similar to Eq. (9).

Graciano and Ayestarán (2013) investigated the nonlinear behavior of unstiffened girder webs subjected to combined concentrated loading, bending, and shear stress using the finite element method. They showed that the bending action is the most influential factor to cause a reduction in patch loading resistance. Finally, Kövesdi et al. (2014) updated the interaction equation derived by Braun (2010) through statistical analysis. Different plate geometries were considered in the investigation and the results showed that the flange greatly influences the design equation:

$$\left(\frac{M}{M_{\mathrm{pl,R}}}\right)^{3.0}+\left(\frac{V-0.5\cdot F}{V_{\mathrm{R}}}\right)^{1.6}+\left(\frac{F}{F_{\mathrm{R}}}\right)\le 1, \tag{9}$$

where $M_{\mathrm{pl,R}}$ is the plastic resistance of the cross-section consisting of the effective area of the flanges and the fully effective web irrespective of its section class; F_{R} and V_{R} are the patch loading and shear buckling resistance respectively of the loaded web panel; F is the patch loading.

Maiorana et al. (2008) derived an innovative calculation for the critical buckling coefficient of a steel plate under *M-F* combined load. The investigation omitted the presence of shear buckling. In the present study, new analyses have been performed to take into account the influence of both bending and shear stress in the critical patch loading force. Therefore, the principal aim of the present investigation is to extend the authors' previous work (Maiorana et al., 2008) and the following points will be addressed in detail:

1. Description of the influence of geometrical and load parameters on the critical buckling load multiplier by performing a parametric analysis.

2. Derivation of a new analytical equation through linear FEM analysis to obtain the critical

buckling load factor $\lambda_{cr,M+V+F}$ of a steel plate under combined *M*-*V*-*F* load.

3. Derivation of the critical patch loading buckling coefficient $k^F_{cr,F+M+V}$ to estimate the critical patch loading of a steel plate subjected to combined *M*-*V*-*F* loads.

4. Presentation of a practical design case with a specific geometry currently used in the bridge industry to show the applicability of the derived equation.

3 Finite element analysis

The elastic stability of a rectangular steel plate subjected to combined patch loading, bending, and shear stress is studied through finite element analysis using Strand 7 (2005). Shell elements with four nodes, Quad 4, and six degrees of freedom are used in the analysis. The material is considered linear elastic since linear buckling is to be performed.

Constraint in the *z*-direction has been applied along the four sides of the plate to avoid out-of-plane displacement. At each corner node, elastic restraint with a specific stiffness is applied to allow the corner nodes to move in the *x*- and *y*-directions. In order to keep the direction of the load fixed in the deformed shape of the plate, it is directly applied to each node as a system of conservative forces.

In order to validate the numerical results, two calibrations were carried out. In the calibration process, a steel plate with the characteristics presented in Table 1 and displayed in Fig. 1a is considered. At the first stage, it was necessary to define an appropriate beam element with a specific elastic restraint (Table 2) giving FEM results close to the results from the literature. The steel plate under combined patch loading and bending stress was analyzed and the numerical results were compared to Maiorana et al. (2008) and they showed a good agreement with a maximum difference equal to 2.9% as presented in Table 3.

Table 1 Characteristics of material and section tested for calibration

E (N/mm^2)	v	a (mm)	t (mm)	b (mm)
206 000	0.3	2000	10	1000

E: Young's modulus; *v*: Poisson's ratio; *b*: height of the steel plate (height of the steel web); *t*: thickness of the steel plate (thickness of the steel web)

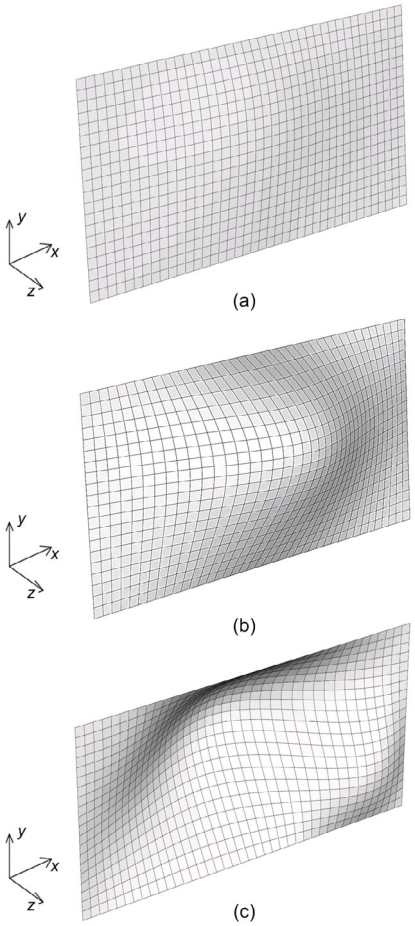

Fig. 1 Numerical model in the calibration phase
(a) Flat steel plate; (b) Buckling shape of steel plate under patch loading; (c) Buckling plate of steel plate under combined patch loading and bending moment

Table 2 Geometry and mechanical characteristics of elastic restraint

Diameter (mm)	L (mm)	E (MPa)	EA'/L (N/mm)
3	300	206 000	4853.76

A' is the section, L is the length of the elastic restraint, and EA'/L is the axial stiffness of the elastic restraint

The second calibration concerns the accuracy of the mesh. A steel plate with the same characteristics presented in Table 1 subjected to patch loading was studied and the numerical results are compared with the results of previous studies. A good correlation is found in accordance with previous results as presented in Table 4. In Figs. 1b and 1c, the first buckling mode of the steel plate under patch loading and combined patch loading and bending moment are presented, respectively, whereas in Fig. 2, the typical loading scheme and boundary conditions of the model

investigated in the next parts of the study are presented.

Table 3 Calibration of the elastic restraints (F=100 kN)

ψ	Method	λ_{cr}		
		σ_0=10 MPa	σ_0=50 MPa	σ_0=100 MPa
−1	Maiorana et al., 2008	4.23	3.53	2.79
	FEM	4.23	3.54	2.81
	Δ	0.0%	0.3%	0.7%
−0.5	Maiorana et al., 2008	3.99	2.83	2.01
	FEM	3.98	2.83	2.02
	Δ	0.3%	0.0%	0.5%
0	Maiorana et al., 2008	3.76	2.27	1.36
	FEM	3.75	2.27	1.40
	Δ	0.3%	0.0%	2.9%
1	Maiorana et al., 2008	3.34	1.41	0.71
	FEM	3.33	1.45	0.73
	Δ	0.3%	2.8%	2.8%

λ_{cr} is the critical buckling factor for combined patch loading and bending, Δ is the relative difference between the FEM results and the result from Maiorana et al. (2008), and ψ is the bending stress ratio

Table 4 Buckling coefficients of plate under patch loading only (a/b=2)

l_0/a	$k_{F,FEM}$	k_F			
		Alinia, 2005	Shahabian and Roberts, 1999	Graciano and Lagerqvist, 2003	Ren and Tong, 2005
0.0	3.31	3.25	–	3.23	3.22
0.1	3.39	3.30	3.27	3.26	–
0.2	3.51	3.45	–	3.34	3.36
0.3	3.68	3.60	–	3.49	3.51
0.4	3.90	3.70	3.68	3.67	3.71
0.5	4.17	3.95	3.90	3.92	3.97

$k_{F,FEM}$ is the critical buckling coefficient from FEM analyses of a steel plate under patch loading, k_F is the critical buckling coefficient of a steel plate under patch loading found in the literature, σ_0 is the maximum normal stress, and l_0 is the patch loading length

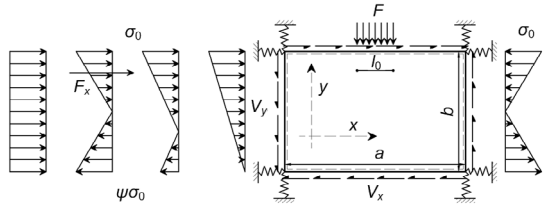

Fig. 2 Plate subjected to combined patch loading, bending, and shear

In regards to the loading configuration, the bending stresses with different stress ratios (ψ=−1, ψ=−0.5, ψ=0, and ψ=1) are applied in the x-direction where the magnitudes are chosen according to current observations of a real project as highlighted by Maiorana et al. (2008). However, only the compressive part of the bending stress will be considered since it is relevant in the buckling analysis. In Eqs. (10)–(12), the existing relationship between patch loading, bending moment, and shear force is presented.

$$F_x=A\cdot F, \tag{10}$$

$$V_y=B\cdot F_x=B\cdot A\cdot F, \tag{11}$$

$$V_x=\frac{a}{b}\cdot V_y=\frac{a}{b}\cdot B\cdot A\cdot F, \tag{12}$$

where the coefficients A and B represent the loading parameters which describe the relationship between different in-plane loadings and are defined in Table 5. V_x and V_y are the equivalent shear force in the horizontal and vertical directions, respectively. F_x represents the integral of the compressive part of the bending stress and can be obtained:

$$F_x=\begin{cases}\sigma_0\dfrac{b\cdot t}{4}, & \psi=-1,\\ \sigma_0\dfrac{2b\cdot t}{3}, & \psi=-0.5,\\ \sigma_0\dfrac{b\cdot t}{2}, & \psi=0,\\ \sigma_0\cdot b\cdot t, & \psi=1,\end{cases}$$

where σ_0 is the maximum normal stress, b is the height of the steel plate, and t is the plate's thickness.

In theory, there is no mathematical relationship between patch loading F and the resulting compressive force F_x obtained from the bending moment. The loading parameters have been chosen with the aim to match as close as possible to real cases whereas a and b are related to the geometrical characteristics of the steel plate.

$$V_x=\int\tau_{xy}\,\mathrm{d}A', \tag{13}$$

$$V_y=\int\tau_{yx}\,\mathrm{d}A', \tag{14}$$

where τ_{xy} and τ_{yx} represent the shear stresses in the y and x directions, respectively as shown in Fig. 3.

Since $\tau_{xy}=\tau_{yx}$, τ_{xy} is supposed to be constant along edge b and τ_{yx} is supposed to be constant along side a, Eqs. (13) and (14) will become, respectively, Eqs. (15) and (16).

$$V_x=\tau_{xy}\cdot a\cdot t, \tag{15}$$

$$V_y=\tau_{yx}\cdot b\cdot t. \tag{16}$$

Table 5 Parameters taking into consideration in the FEM analysis

A	B	ψ	F (kN)	a/b	b/t	l_0/a
2.0	1/5	−1.0	100	1.0	50	0.0
2.5	2/5	−0.5	200	1.5	100	0.1
3.0	3/5	0.0	300	2.0	150	0.2
3.5	4/5	1.0	400	2.5	200	0.3
4.0	5/5		500	3.0	250	0.4
						0.5

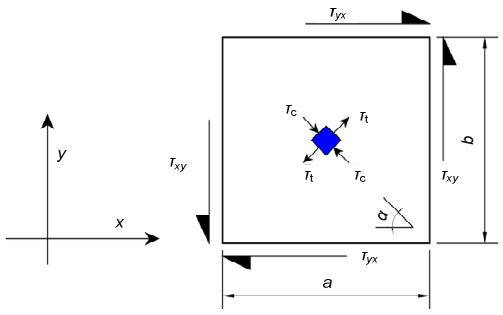

Fig. 3 Plate under a pure shear
τ_c and τ_t are respectively the internal diagonal compression and tension stresses involved in the shear mechanism

4 Parametric studies

Several parameters may influence the stability of a steel plate under in-plane combined loading conditions. The patch loading length, the patch loading magnitude, the panel aspect ratio, and the plate's slenderness defined as the plate's height-to-thickness ratio are the most important since many researchers (Alinia, 2005; Maiorana et al., 2008; Loaiza et al., 2017) have focused their research on either one or a couple of them. In this section, the influence of each parameter will be studied through the following strategy.

4.1 Research strategy

The plate's geometry corresponds to one of the most important parameters in the parametric analysis of the buckling of steel plates. The geometry is chosen based on current real-world situations. A steel plate with the following geometry was considered: a=1000 mm, b=1000 mm, and t=10 mm. Then, to consider different situations, the geometrical parameters such as the panel aspect ratio a/b and the plate's slenderness b/t are varied. The geometrical parameters considered starting from the initial plate's geometry are the following: a/b=1, 1.5, 2, 2.5, 3, b/t=50, 100, 150, 200, 250.

At the first step, the steel plate subjected to patch loading was studied carefully. For each geometrical configuration, different patch loading magnitudes of different lengths were applied. Then shear force and bending stress through their equivalent compressive force were added to the model to consider the interaction of the three in-plane loadings. For the added shear and bending forces, patch loading F was incremented from 100 kN to 500 kN and the l_0/a parameter from 0.0 to 0.5.

4.2 Investigation of a steel plate under *M-F-V* interaction

A steel plate subjected to in-plane loading interactions may behave differently according to the loading which is applied: bending, shear or patch loading. Considering the interaction of the stresses generated by each force, the worst case for the steel plate is always observed when the bending stress acting on it has a stress ratio ψ=0 because this condition adds more compressive stress in the plate. However, the plate will be less prone to instability for ψ=−1 as seen in Fig. 4.

4.2.1 Influence of patch loading length and panel aspect ratio

Several analyses showed that the critical buckling load of a plate subjected to combined in-plane loadings will increase and the patch loading length will increase as well (Fig. 4a). The same conclusion cannot be drawn for the variation of the panel aspect ratio. In fact, Fig. 4b shows that the critical buckling load multiplier goes slightly down by increasing the panel aspect ratio for the case of ψ=−1 while it will slightly increase and decrease alternately for other stress ratios. The critical buckling load will depend on

the number of half-waves induced by the deformation of the plate and consequently on the length of the half-wave.

Besides the mechanical characteristics of the material and the parameters of the structural elements able to modify the stress state, the intensity of the patch loading, bending, and shear force is clearly important in the plate stability. In fact, patch loading applied in a small beam portion will increase the instability process of the beam. In addition, in the situation where the section is also subjected to both bending and shear forces, the instability will happen at an early stage. For different lengths of patch loading, the instability is more sensitive to the bending variation with respect to the shear's variation. Fig. 5 shows that considering a maximum value of bending stress interacting with different levels of shear force, the critical buckling load decreases at a slow rate.

When the bending stress is increasing gradually, the plate goes to instability faster as a steeper slope describes the variation of the critical buckling stress. In addition, it can be seen in Fig. 6 (p.398) that the variation of bending or shear forces generates a greater impact on the critical buckling load multiplier with respect to the variation of the panel aspect ratio. This conclusion is validated by observing the slight variation of the load multiplier as a function of the panel aspect ratio in Fig. 4b.

4.2.2 Influence of patch loading magnitude and plate's slenderness

With respect to the impact of slenderness and patch loading magnitude (Figs. 4c and 4d), the conclusion for the steel plate subjected to combined loading is similar to the case of the plate under a single load type. Slender plates will have higher

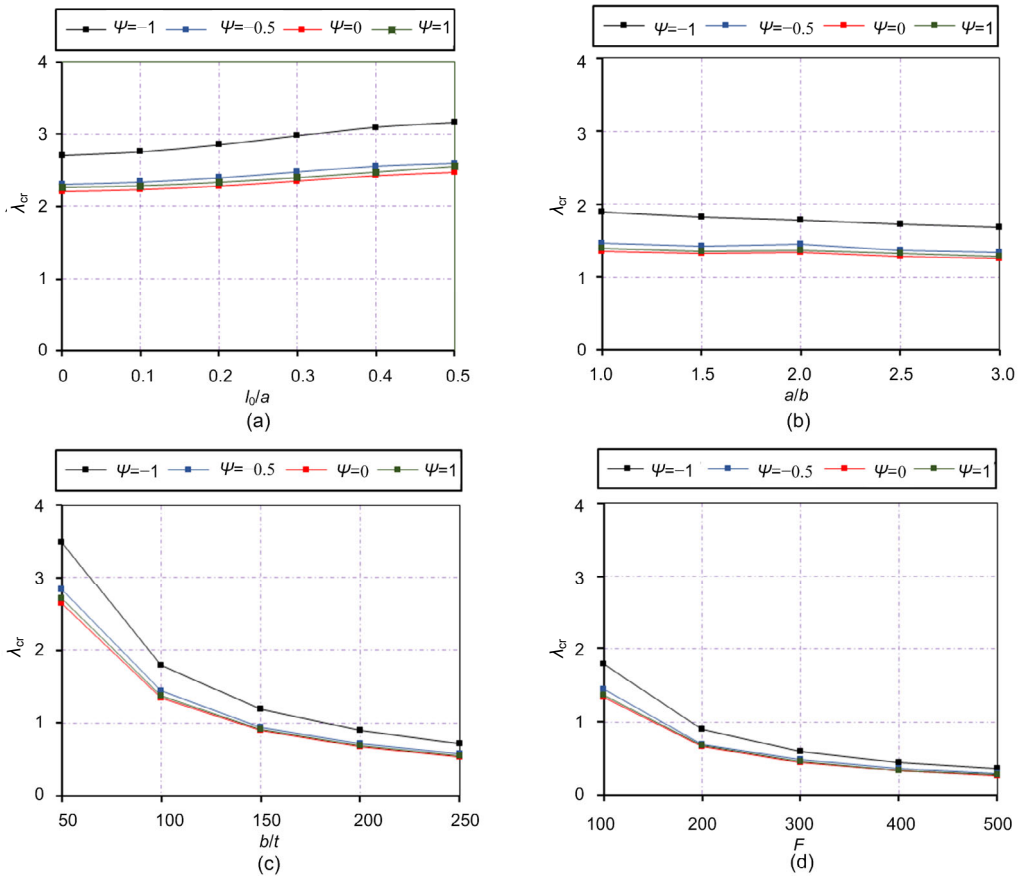

Fig. 4 Variation of the critical buckling load factor for steel plate section subjected to combined patch loading, bending, and shear force: F=100 kN; F_x=4F; V_y=F_x

(a) Influence of patch loading length; (b) Influence of the panel aspect ratio; (c) Influence of the slenderness; (d) Influence of the patch loading magnitude. The four lines, from top to bottom, represent ψ=−1, −0.5, 1, and 0, respectively

exposure to buckling than compact steel plates. Meanwhile, a steel I-profile bridge girder will undergo instability faster if the reaction at the support pillar is high.

It is worth noting that the critical buckling stress of the plate subjected to combined loading when the patch loading magnitude rises is interconnected while the level of bending and shear stresses defined by A and B, respectively, remains the same. The patch loading, in this case, governs the buckling mode and the plate behaves exactly as if it were subjected to only patch loading.

Contrary to what has been observed in Figs. 5 and 6, the patch loading magnitude and the

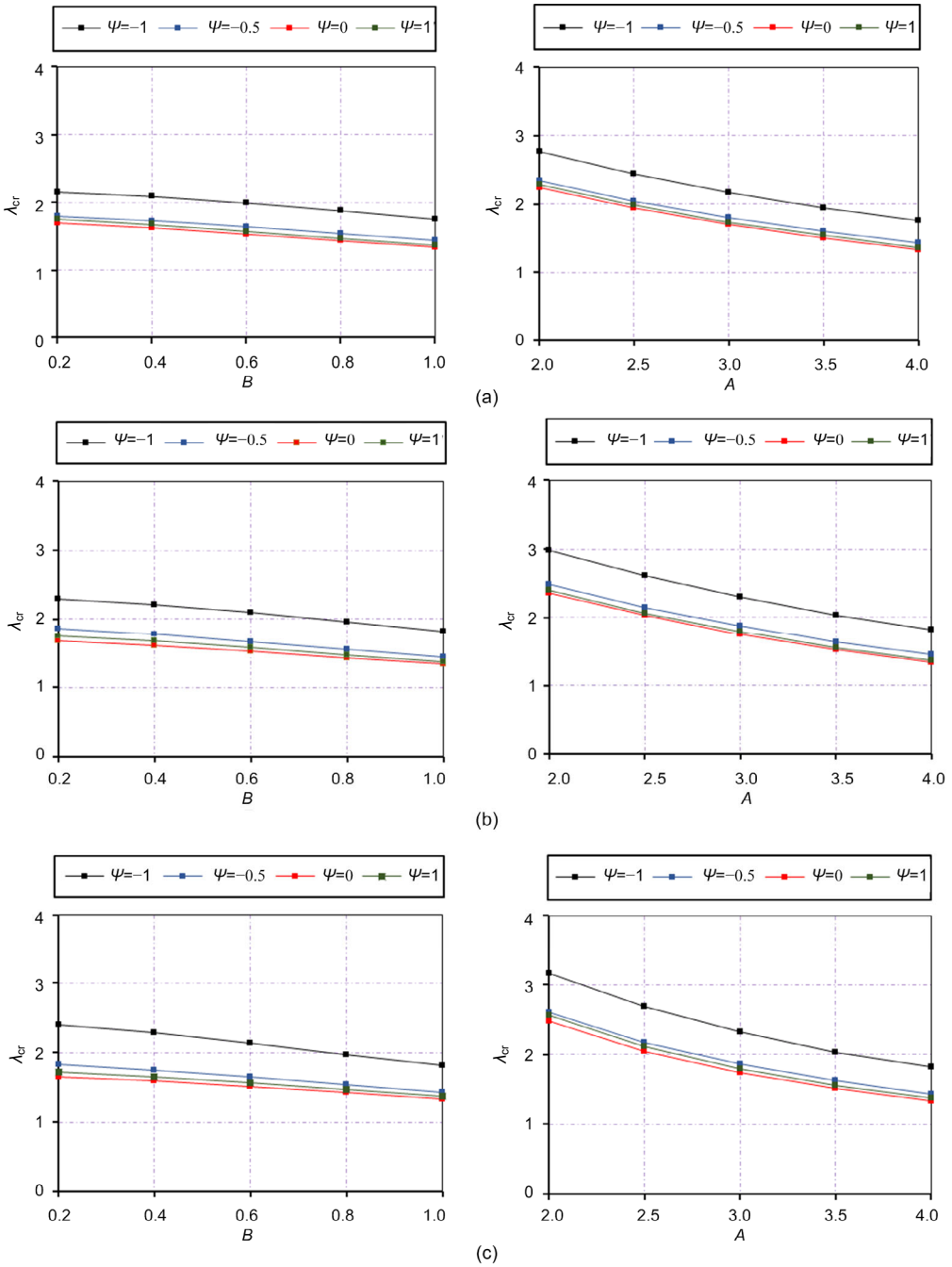

Fig. 5 Influence of patch loading length in the critical buckling load multiplier: (a) l_0/a=0.1; (b) l_0/a=0.3; (c) l_0/a=0.5
The four lines, from top to bottom, represent ψ=−1, −0.5, 1, and 0, respectively

slenderness of the steel plate greatly influence the critical buckling load (Figs. 7 and 8). In particular, the slenderness of the steel plates is considered the critical parameter (Fig. 8) leading to the plate's instability because it is the unique parameter that strongly influences the critical buckling load multiplier. It is worth noting that as the patch loading magnitude is increased, the increase of shear stress will change the critical load from a slight reduction to a quasi-constant value (Fig. 7).

4.3 Failure mode of a steel plate under combined in-plane loadings

Steel plates under loads may present different

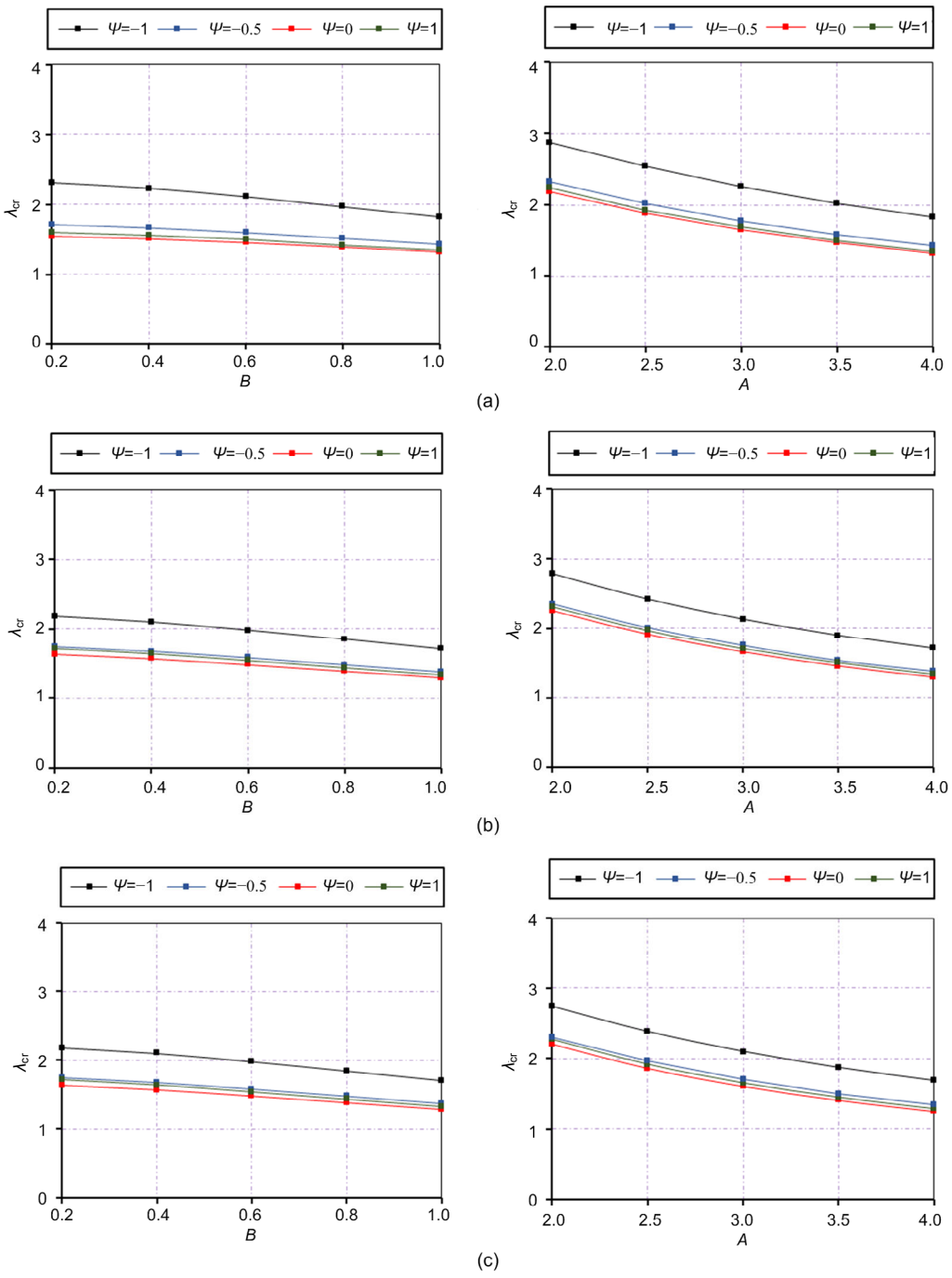

Fig. 6 Influence of panel aspect ratio α in the critical buckling load multiplier: (a) α=1.5; (b) α=2.5; (c) α=3.0
The four lines, from top to bottom, represent ψ=−1, −0.5, 1, and 0, respectively

buckling shapes depending on the type of loads and the geometrical parameters. When dealing with plates under combined loads, the buckling shape of the plate can be described in general in four ways as shown in Fig. 9 (p.401).

If the shear force is significantly low with respect to both bending and patch loading and in the meantime, the patch loading is dominant in relation to bending, the buckling shape of the plate will be similar to the case of the plate under patch loading (Fig. 9a). The plate will display a deformation following the direction of patch loading. From the moment that the bending stress is increasing up to the point that it is dominant in relation to patch loading,

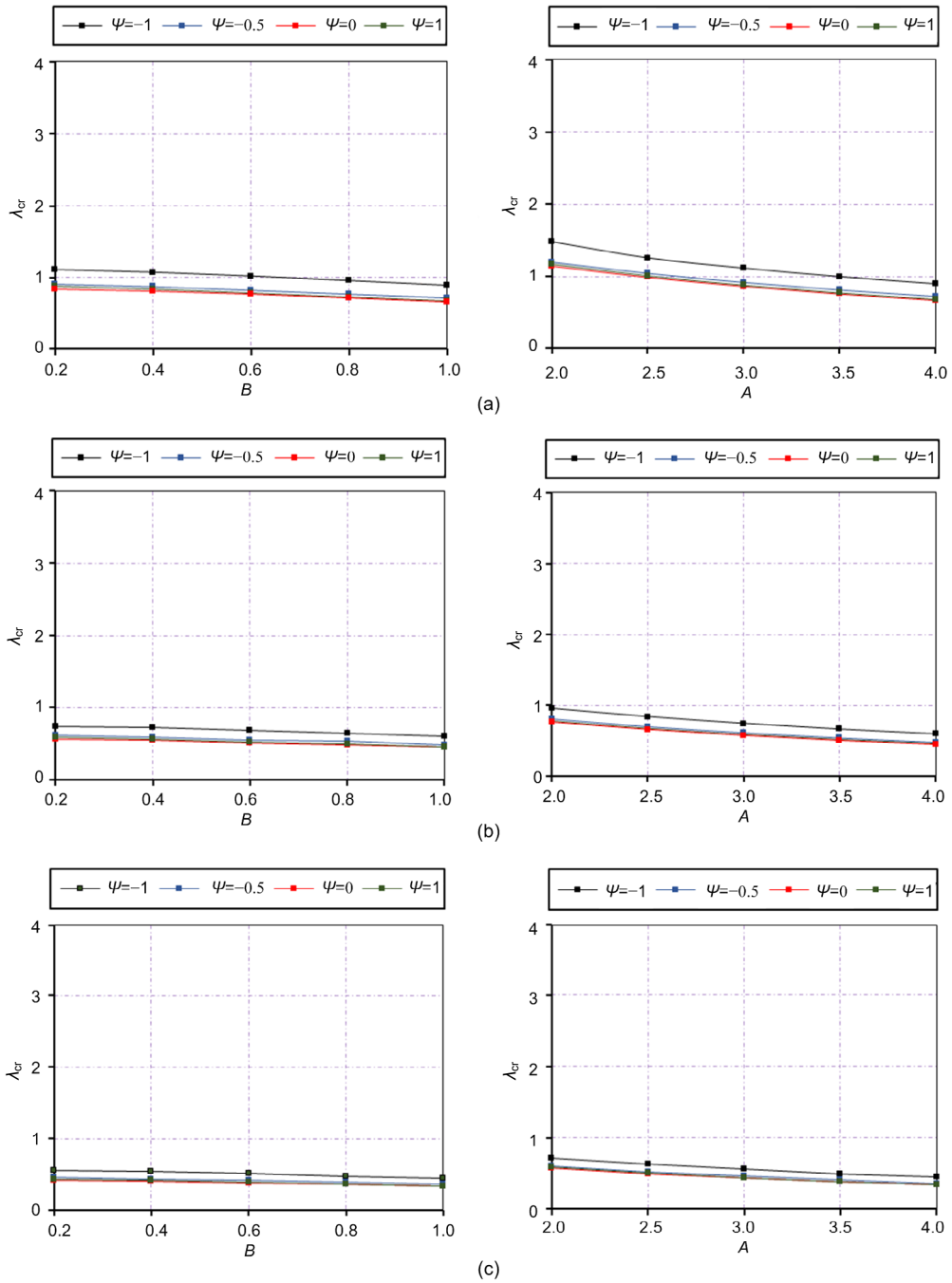

Fig. 7 Influence of patch loading magnitude in the critical buckling load multiplier: (a) F=200 kN; (b) F=300 kN; (c) F=400 kN. The four lines, from top to bottom, represent ψ=−1, −0.5, 1, and 0, respectively

the deformation shape will then follow the direction of bending with the number of half-wave functions to the plate's geometry and constraint condition as shown in Figs. 9b and 10b.

Finally, if the shear is increased in the same mode as the bending moment, the situations in Figs. 9b, 9c, 10a, and 11 will be observed. A tension field inclined at a certain angle with respect to the horizontal will be gradually developed following the diagonal of the plate in the case of one half-wave as shown in Fig. 9c or the diagonal of each tension field created in the case of multiple wavelengths will be as shown in Figs. 10a and 11.

It is interesting to add that the patch loading

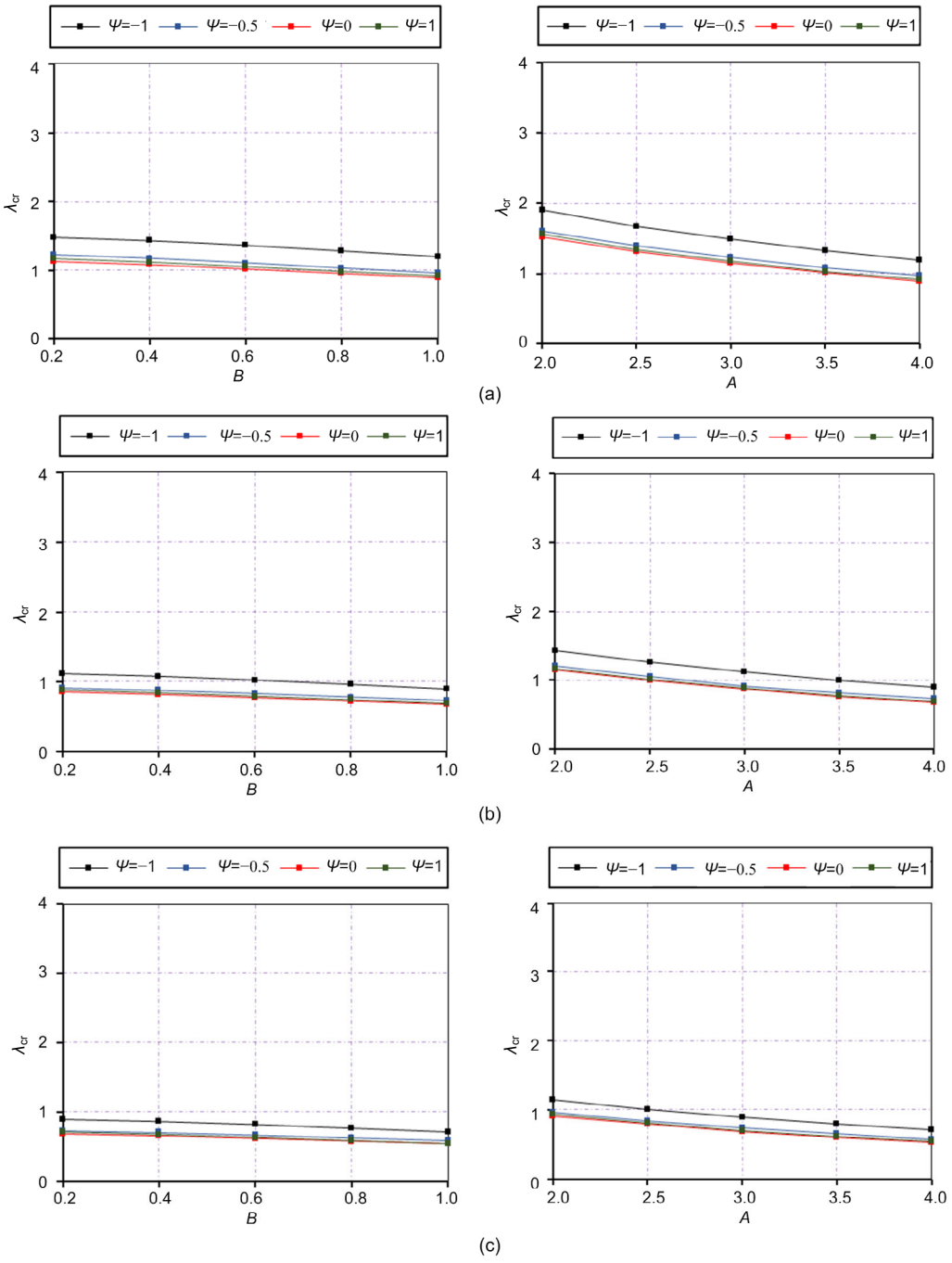

Fig. 8 Influence of slenderness in the critical buckling load multiplier: (a) *b*/*t*=150; (b) *b*/*t*=200; (c) *b*/*t*=250
The four lines, from top to bottom, represent ψ=−1, −0.5, 1, and 0, respectively

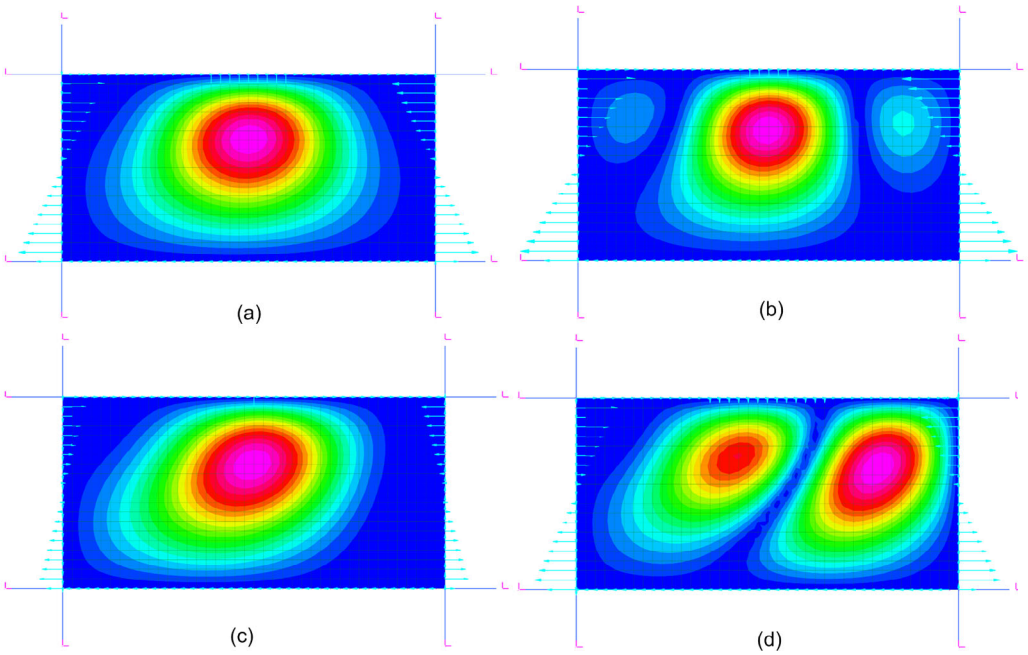

Fig. 9 Critical buckling shape of plate under patch loading, bending and shear, varying patch loading length
(a) l_0/a=0.2; (b) l_0/a=0.1; (c) l_0/a=0; (d) l_0/a=0.3

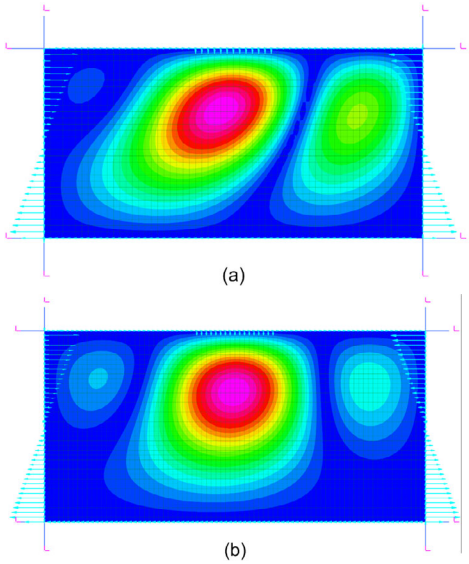

Fig. 10 Critical buckling shape of plate under patch loading, bending and shear, varying slenderness
(a) b/t=150; (b) b/t=200

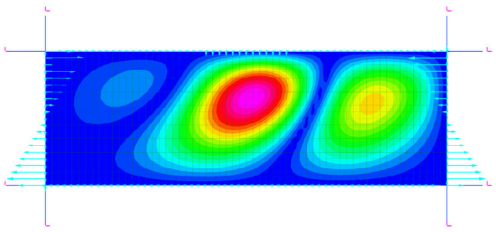

Fig. 11 Critical buckling shape of plate under patch loading, bending, and shear for aspect ratio a/b=3

length can in some cases influence the buckling shape. Figs. 9c and 9d present two plates' deflections observed for the same state of loading. When the patch loading is very small, it will lead to one wave-deformed shape and then the situation will progressively change as well as the patch loading length increases.

5 Elastic critical buckling of a steel plate under *M-F-V* interaction

The elastic critical buckling of a steel plate subjected to patch loading F can be obtained by theory as described in (Timoshenko and Woinowsky-Krieger, 1959) or using FEM analysis. When the theory is used, it is necessary to know the critical buckling coefficient, which is found in the literature since several researchers have worked on the topic (Timoshenko and Woinowsky-Krieger, 1959; Duchene and Maquoi, 1994; Ren and Tong, 2005; Maiorana et al., 2008) while from the numerical analysis, the critical buckling load factor is expected. Eq. (17) defines the relationship between the approaches. Therefore, it is possible to find the buckling load multiplier for a steel plate under patch loading throughout Eq. (18) knowing the geometrical

characteristics of the steel plate, the patch loading, and the critical buckling coefficient.

$$F_{\mathrm{cr},F} = k_F \times \frac{\pi^2 E t^3}{12(1-\nu^2)b} = \lambda_{\mathrm{cr},F} \times F, \tag{17}$$

$$\lambda_{\mathrm{cr},F} = k_F \times \frac{\pi^2 E t^3}{12(1-\nu^2)b} \Big/ F, \tag{18}$$

where $\lambda_{\mathrm{cr},F}$ is the critical buckling load multiplier of the steel plate subjected to patch loading; k_F is the critical buckling coefficient of the steel plate subjected to patch loading; $F_{\mathrm{cr},F}$ is the critical patch loading force of the steel plate.

5.1 Research strategy

In this section, the equations in terms of parameters from Table 5 that describe the influence of bending and shear forces in the critical buckling load are proposed. In the previous section, it was possible to observe that these parameters influenced in some way the critical buckling load factors of steel plate subjected to the interaction of in-plane loading. On the other hand, the critical buckling load factors do not evolve linearly with the geometrical and loading parameters investigated in the previous section. For this reason, each parameter will be studied separately. To reach our goal the following strategy is adopted.

A steel plate with the following geometry a=2000 mm, b=1000 mm, t=10 mm is considered. In the first step, the patch loading with different configurations of load length is applied to the steel plate whereas the shear force and bending moment are varied through the A and B coefficients. Table 6 shows the different fixed and varying parameters considered in the first step. For each combination of variables presented in Table 6, the buckling load factors are computed, hence over 500 numerical models were investigated in this step. The results from the analysis lead to discovery of a unique function in terms of load parameters A and B and patch loading length l_0/a, which accurately describes the reduction of critical buckling loads.

In the next steps, the other parameters such as patch loading magnitude, panel aspect ratio, and the plate's slenderness will be investigated one at a time. However, it is worth noting that the following plate geometries, a=2000 mm, b=1000 mm, t=10 mm, and the patch loading length l_0/a=0.2, are the benchmark for the analysis. In the variation of panel aspect ratio, only the length of the plate is changed whereas when the slenderness is varied, both the length and the height of the plate are involved to keep the panel aspect ratio fixed to 2. The shear force and bending moment are varied through the A and B coefficients similarly to the previous analysis. Thus, over 400 numerical models were investigated for each parameter involved and the influence of shear force and bending moment in the reduction of the buckling loads factor can be derived. The design equation will be proposed with the aim to match it as close as possible to the different values from the FEM analysis. Therefore, the comparison of values from the design formula and FEM calculations was done to assess in some way the uncertainty of the design parameters. In order to limit the deviation as much as possible, a maximum error of ±5% was fixed between the different values compared.

Table 6 Parameters used to determine the critical buckling load factor

a/b	b/t	F (kN)	A	B	l_0/a
2	100	100	2.0	1/5	0.0
			2.5	2/5	0.1
			3.0	3/5	0.2
			3.5	4/5	0.3
			4.0	5/5	0.4
					0.5

5.2 Evaluation of the buckling load factor

By reworking the data set obtained from numerical analysis, a critical buckling load factor, which takes into account the interaction of patch loading with both shear and bending forces, has been defined. The relationship derived and expressed in Eqs. (19) and (20) in terms of A and B parameters allows us to determine how the additional forces lower the critical buckling load. The P_{ij} coefficients are determined through a regression fitting analysis and are influenced by the parameters investigated. For this reason, these coefficients have been defined accordingly to the involved parameter. It is worth noting that the equations are applicable to within a specific range of the plate's geometry and the loading cases that have been considered in the analysis and this range is

presented in Table 7. On the other hand, users should first identify the geometrical and loading characteristics of the problem. Then, with the design parameters, they will be able to determine which equations should be used.

$$\frac{\lambda_{\mathrm{cr},F}}{\lambda_{\mathrm{cr},M+F+V}} = f(A,B), \tag{19}$$

$$\frac{\lambda_{\mathrm{cr},F}}{\lambda_{\mathrm{cr},M+F+V}} = P_{20}\cdot A^2 + P_{02}\cdot B^2 + P_{11}\cdot A\cdot B + P_{10}\cdot A + P_{01}\cdot B + P_{00}, \tag{20}$$

where P_{ij} are polynomial coefficients depending on the geometrical and loading characteristics (patch loading length, patch loading magnitude, panel aspect ratio, and plate slenderness λ).

5.2.1 Influence of patch loading length

Through Matlab (2017)'s tools, a 3D chart describing the variation of the critical buckling load multiplier of the steel plate involved in the first step is drawn. We recall that in this case, only shear forces, bending moment, and patch loading length are varied. Then using the regression fitting curve analysis, the P_{ij} coefficients are obtained as a function of the patch loading length (Table 8).

Over 500 numerical results have been assessed and compared to the design formula. The comparison between FEM analysis and analytical equations showed a good agreement in this case. Checks were done separately for each bending stress ratio. All the values compared are located inside the limits imposed as shown in Fig. 12.

Table 7 Range of applicability of the design formula

F_x (kN)	V_y (kN)	l_0/a	λ	α
[2F, 4F]	[0.2F_x, F_x]	[0, 0.5]	100	2
[2F, 4F]	[0.2F_x, F_x]	0.2	100	2
[2F, 4F]	[0.2F_x, F_x]	0.2	[50, 250]	2
[2F, 4F]	[0.2F_x, F_x]	0.2	100	[1, 3]

Table 8 Design coefficients used in case of patch loading length as parameter

Parameter	ψ=−1,	ψ=−0.5,	ψ=0,	ψ=1,
	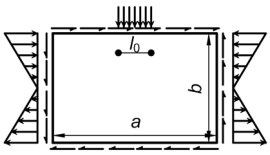	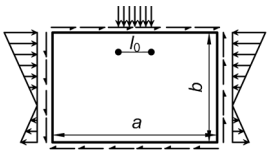	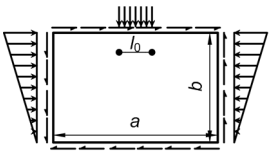	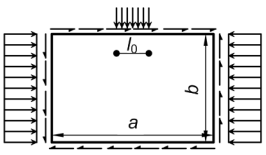
P_{00}	$-0.391\left(\frac{l_0}{a}\right)+1.145$	$-0.593\left(\frac{l_0}{a}\right)+1.362$	$-1.018\left(\frac{l_0}{a}\right)+1.485$	$-0.603\left(\frac{l_0}{a}\right)+1.405$
P_{10}	$0.196\left(\frac{l_0}{a}\right)+0.107$	$0.380\left(\frac{l_0}{a}\right)+0.112$	$0.703\left(\frac{l_0}{a}\right)+0.050$	$0.438\left(\frac{l_0}{a}\right)+0.067$
P_{01}	$-0.329\left(\frac{l_0}{a}\right)-0.453$	$0.001\left(\frac{l_0}{a}\right)-0.673$	$0.158\left(\frac{l_0}{a}\right)-0.721$	$0.035\left(\frac{l_0}{a}\right)-0.705$
P_{11}	$0.179\left(\frac{l_0}{a}\right)+0.163$	$0.160\left(\frac{l_0}{a}\right)+0.244$	$0.013\left(\frac{l_0}{a}\right)+0.289$	$0.022\left(\frac{l_0}{a}\right)+0.300$
P_{20}	$0.022\left(\frac{l_0}{a}\right)+0.023$	$0.033\left(\frac{l_0}{a}\right)+0.029$	$0.014\left(\frac{l_0}{a}\right)+0.043$	$0.049\left(\frac{l_0}{a}\right)+0.037$
P_{02}	$0.431\left(\frac{l_0}{a}\right)+0.260$	$0.197\left(\frac{l_0}{a}\right)+0.332$	$0.266\left(\frac{l_0}{a}\right)+0.320$	$0.304\left(\frac{l_0}{a}\right)+0.317$

5.2.2 Influence of patch loading magnitude

The patch loading magnitude is another parameter involved in the analysis as defined in the research strategy. By reworking the numerical results obtained from analysis, the 3D charts from Matlab (2017) showed that the patch loading magnitude considered in Table 5 does not influence Eq. (20) since the ratio gives the same value for each patch loading magnitude (Fig. 13). For this reason, the coefficients P_{ij} are easily found and are constants. Table 9 presents different values for P_{ij} coefficients found after a regression fitting of the 3D charts.

5.2.3 Influence of the plate's slenderness

Similar to the case of patch loading magnitude, the same observation has been made by analyzing the numerical results through a 3D chart. In fact, even if the variation of plate slenderness influences the critical loading in the case of combined in-plane loading, the ratio described in Eq. (19) remains constant. For this reason, the coefficients P_{ij} are easily found and are not a function of the slenderness. Table 10 presents different values for P_{ij} coefficients found after a regression fitting of the 3D charts.

5.2.4 Influence of the panel aspect ratio

Panel aspect ratio is the plate's parameter that did not present a specific conclusion. Indeed, the elaboration of P_{ij} coefficients in the case of varying the panel aspect ratio encountered some difficulties since the convergence was difficult to reach. For this reason, P_{ij} coefficients are defined in this case as a polynomial equation of grade 3 as presented in Table 11.

The comparison of numerical results and analytical equations showed good agreement with the maximum deviation equal to 5% when the patch loading length, the patch loading magnitude, and the plate's slenderness were considered separately. On the other hand, when the panel aspect ratio was involved the results presented large deviation especially when there were long plates. Nevertheless, the results are acceptable with the maximum observed deviation up to

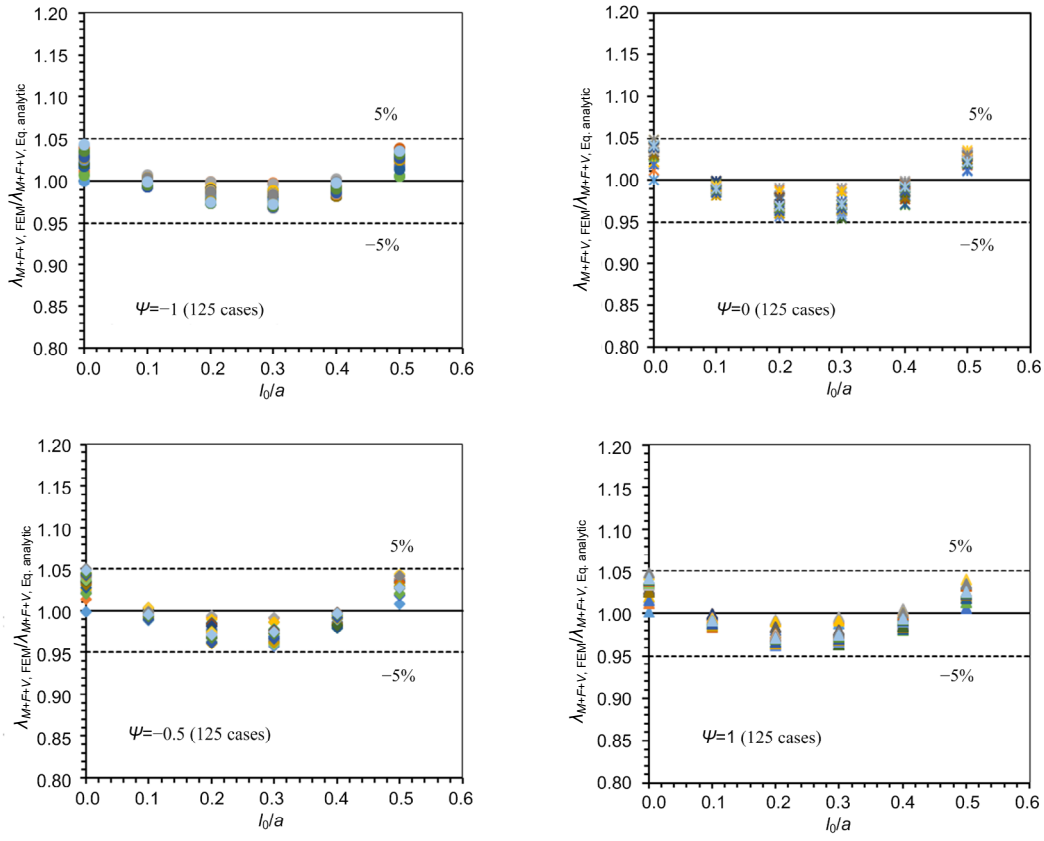

Fig. 12 Comparison between FEM and design formula considering the patch loading length

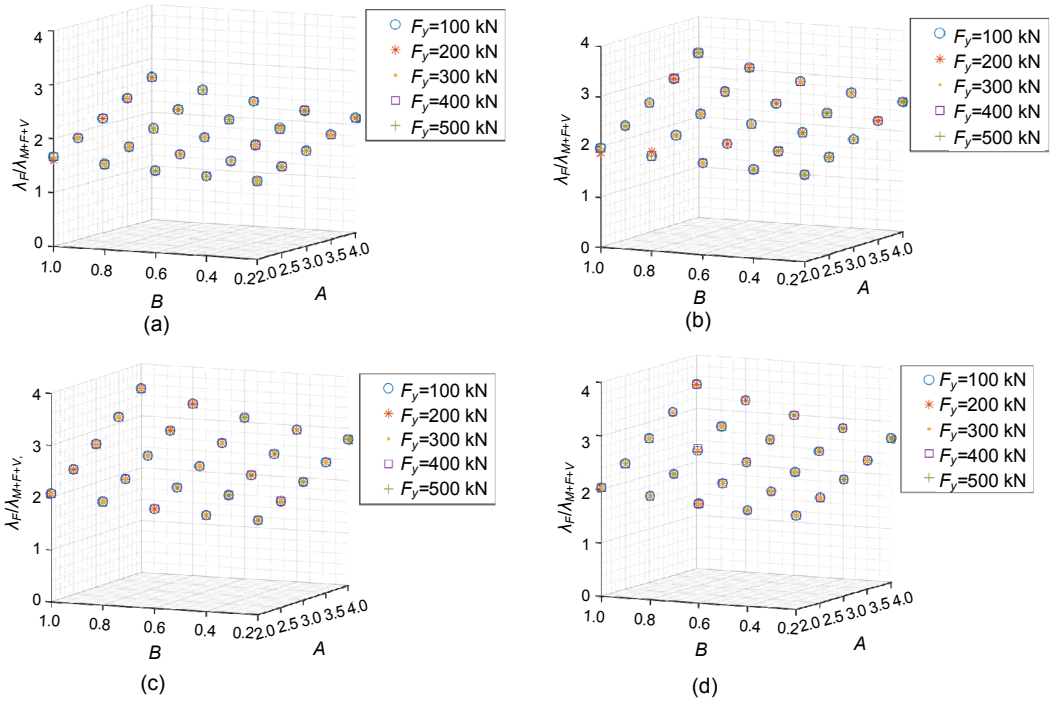

Fig. 13 3D evolution of the critical buckling load multiplier ratio in term of patch loading magnitude
(a) ψ=−1; (b) ψ=−0.5; (c) ψ=0; (d) ψ=1

Table 9 Design coefficients used in case of patch loading magnitude as parameter

ψ	P_{00}	P_{10}	P_{01}	P_{11}	P_{20}	P_{02}
−1	1.086	0.139	−0.515	0.196	0.026	0.318
−0.5	1.306	0.159	−0.703	0.275	0.034	0.371
0	1.451	0.081	−0.728	0.304	0.056	0.362
1	1.385	0.090	−0.706	0.311	0.050	0.358

Table 10 Design coefficients used in case of plate slenderness as parameter

ψ	P_{00}	P_{10}	P_{01}	P_{11}	P_{20}	P_{02}
−1	1.088	0.137	−0.507	0.191	0.026	0.325
−0.5	1.296	0.163	−0.698	0.277	0.033	0.369
0	1.450	0.083	−0.737	0.307	0.055	0.362
1	1.384	0.090	−0.713	0.311	0.050	0.364

Table 11 Design coefficients used in case of panel aspect ratio as parameter

ψ	P_{00}	P_{01}	P_{10}	P_{11}	P_{20}	P_{02}
−1	$0.239\alpha^3-1.476\alpha^2$	$-0.233\alpha^3+1.426\alpha^2$	$-0.243\alpha^3+1.672\alpha^2$	$0.071\alpha^3-0.444\alpha^2$	$0.008\alpha^3-0.066\alpha^2$	$0.077\alpha^3-0.475\alpha^2$
	$+2.744\alpha-0.376$	$-2.777\alpha+1.129$	$-3.646\alpha+2.669$	$+0.894\alpha-0.361$	$+0.159\alpha-0.098$	$+0.978\alpha-0.328$
−0.5	$0.153\alpha^3-1.146\alpha^2$	$-0.060\alpha^3+0.499\alpha^2$	$-0.158\alpha^3+1.292\alpha^2$	$0.022\alpha^3-0.175\alpha^2$	$-0.006\alpha^3+0.015\alpha^2$	$0.006\alpha^3-0.082\alpha^2$
	$+2.555\alpha-0.525$	$-1.319\alpha+0.425$	$-3.294\alpha+2.900$	$+0.478\alpha-0.155$	$+0.025\alpha-0.036$	$+0.323\alpha+0.011$
0	$0.098\alpha^3-0.917\alpha^2$	$-0.045\alpha^3+0.419\alpha^2$	$-0.083\alpha^3+0.918\alpha^2$	$-0.007\alpha^3-0.018\alpha^2$	$-0.016\alpha^3+0.067\alpha^2$	$0.026\alpha^3-0.177\alpha^2$
	$+2.382\alpha-0.608$	$-1.197\alpha+0.398$	$-2.799\alpha+2.806$	$+0.235\alpha-0.057$	$-0.058\alpha-0.009$	$+0.442\alpha-0.013$
1	$0.089\alpha^3-0.884\alpha^2$	$-0.048\alpha^3+0.447\alpha^2$	$-0.053\alpha^3+0.717\alpha^2$	$-0.016\alpha^3+0.032\alpha^2$	$-0.016\alpha^3+0.073\alpha^2$	$0.039\alpha^3-0.265\alpha^2$
	$+2.407\alpha-0.752$	$-1.275\alpha+0.474$	$-2.395\alpha+2.549$	$+0.141\alpha+0.003$	$-0.073\alpha+0.018$	$+0.629\alpha-0.137$

10%. Table 12 briefly summarizes a comparison between FEM and analytical results of the critical buckling load factor for steel plate under combined in-plane loading with different plates and load characteristics.

5.3 Evaluation of the buckling load coefficient

From the previous section, analytical formulas describing the variation of the critical buckling load multiplier for steel plate were developed. These formulas have been derived through parametric analysis considering four relevant parameters influencing the plate buckling. One of the major issues presented by these formulas is the limited range of applicability because, in a real design situation, the four parameters

Table 12 Comparison between FEM results and analytic results in relation to the plate and loading parameters with Δ

a (mm)	b (mm)	t (mm)	l_0/a	α	λ	ψ	F (kN)	F_x (kN)	V_y (kN)	$\lambda_{cr,M+V+F}^{FEM}$	$\lambda_{cr,M+V+F}^{AN}$	Δ (%)
Variation of panel aspect ratio												
1000	1000	10	0.2	1.0	100	0.0	100	250	50	2.129	2.026	5.0
1500	1000	10	0.2	1.5	100	1.0	100	250	250	1.928	1.881	2.4
2000	1000	10	0.2	2.0	100	0.0	100	300	120	2.037	1.945	4.5
2500	1000	10	0.2	2.5	100	−0.5	100	400	320	1.476	1.395	5.4
3000	1000	10	0.2	3.0	100	−1.0	100	300	60	2.610	2.632	0.8
Variation of plate' slenderness												
1000	500	10	0.2	2	50	−1.0	100	200	80	6.409	6.217	3.0
2000	1000	10	0.2	2	100	−0.5	100	350	210	1.857	1.778	4.3
3000	1500	10	0.2	2	150	0.0	100	250	150	1.459	1.415	3.1
4000	2000	10	0.2	2	200	1.0	100	400	400	0.640	0.688	7.5
5000	2500	10	0.2	2	250	−1.0	100	300	240	0.950	0.916	3.6
Variation of patch loading magnitude												
2000	1000	10	0.2	2	100	−0.5	100	250	200	2.206	2.131	3.4
2000	1000	10	0.2	2	100	0.0	200	600	480	0.920	0.885	3.8
2000	1000	10	0.2	2	100	1.0	300	1050	210	0.658	0.633	3.8
2000	1000	10	0.2	2	100	−1.0	400	800	640	0.749	0.724	6.0
2000	1000	10	0.2	2	100	−0.5	500	2000	1600	0.311	0.300	3.5
Variation of patch loading length												
2000	1000	10	0.0	2	100	−1.0	100	200	200	2.710	2.761	1.9
2000	1000	10	0.1	2	100	−0.5	100	350	70	1.901	1.946	2.4
2000	1000	10	0.2	2	100	0.0	100	250	250	1.979	1.855	6.3
2000	1000	10	0.3	2	100	1.0	100	300	120	2.158	1.945	9.9
2000	1000	10	0.4	2	100	−1.0	100	400	320	1.979	1.787	9.6

$\lambda_{cr,M+V+F}^{FEM}$ and $\lambda_{cr,M+V+F}^{AN}$ represent the critical buckling load factors of the steel plate subjected to interaction patch loading, bending and shear stresses obtained respectively throughout FEM and using formula derived (AN), and Δ is the relative difference between both results

should be associated together and secondly, many engineers prefer to deal directly with critical buckling coefficient to design the buckling resistance of steel plate. For this reason, a single formula to determine the critical plate-buckling load has been proposed. Starting from the previous results of Maiorana et al. (2008), where the critical buckling load of steel plate subjected to patch loading was presented and the formula was updated to take into consideration the effect of bending stress and shear force.

According to the previous research (Maiorana et al., 2008), the critical buckling load of steel plate under patch loading with various lengths is obtained using Eq. (21) where the coefficients c_1 and c_2 defined by Eqs. (22) and (23) are related to the plate geometry and the patch loading length. Finally, it is worth noting that the critical buckling load of steel plate under patch loading can be obtained knowing either the critical buckling coefficient $k_{cr,F}$ or the critical load multiplier λ_{cr}. Both factors are quite different and use a different approach to determine the critical buckling load of a single plate. The main difference is due to the fact that the first factor uses the geometric characteristics of steel plate to find the critical load while the second factor needs the magnitude of the applied patch loading:

$$F_{cr,F}=\left[3.2048\cdot\frac{\pi^2E}{12(1-\nu^2)}\right]\frac{t^3}{b}\cdot\frac{c_1}{c_2}, \tag{21}$$

where c_1 and c_2 are coefficients of reduction of the critical buckling load for steel plate subjected to combined patch loading and bending moment, respectively.

The analysis showed that when dealing with combined in-plane loading, the influence of the patch loading magnitude and the plate's slenderness change

proportionally with the patch loading and the plate geometry, respectively. On the other hand, the panel aspect ratio does not have much influence on the result since we observed a slight variation of the critical buckling load multiplier (as displayed in Fig. 4). For this reason, the new analytical equation describing the change of critical patch loading is strictly dependent on the patch loading length.

$$c_1 = -0.0446\left(\frac{h}{a}\right)^6 + 0.4067\left(\frac{h}{a}\right)^5 - 1.3512\left(\frac{h}{a}\right)^4 + 1.8338\left(\frac{h}{a}\right)^3 - 0.3869\left(\frac{h}{a}\right)^2 - 0.2617\left(\frac{h}{a}\right) + 0.8035, \tag{22}$$

$$c_2 = 1.9774\left(\frac{l_0}{a}\right)^6 - 6.0815\left(\frac{l_0}{a}\right)^5 + 7.1163\left(\frac{l_0}{a}\right)^4 - 3.5774\left(\frac{l_0}{a}\right)^3 + 0.2617\left(\frac{l_0}{a}\right)^2 - 0.1669\left(\frac{l_0}{a}\right) + 1. \tag{23}$$

The new expressions of critical buckling patch loading and critical buckling patch loading coefficient of steel plate subjected to bending, shear, and patch loading acting simultaneously are presented in Eqs. (24) and (25). The coefficient c_4 can be calculated as a function of the patch loading length, the relationship between different solicitations provided by A and B coefficients and will be different according to different stress ratios. Table 13 summarizes the expressions of c_4 for the corresponding stress ratio.

$$F_{\mathrm{cr},F+M+V}^{F} = \left[3.2048 \cdot \frac{\pi^2 E}{12(1-\nu^2)}\right]\frac{t^3}{h}\cdot\frac{c_1}{c_2}\cdot\frac{1}{c_4}, \tag{24}$$

$$k_{\mathrm{cr},F+M+V}^{F} = 3.2048 \cdot \frac{c_1}{c_2}\cdot\frac{1}{c_4}, \tag{25}$$

where c_4 is the coefficient of reduction of the critical buckling load which takes into account the shear force.

6 Design example

In this section, an application is presented to prove the validity of the analytical equations; the aim of this example is firstly to show how the formula can be used in a practical case and on the other hand to compare the analytical result with the FEM result as proof of acceptance.

Considering a case of a twin girder composite bridge in the launching phase, each girder is made by a structural steel double T-section without longitudinal stiffener but with vertical stiffeners equally spaced to each other. Young's modulus of the material is E=206 000 MPa and Poisson's ratio ν=0.3. Fig. 14 shows a typical section of the girder under study subjected to combined bearing reaction, bending moment, and shear stress. The information provided shows that the plate representing the web girder is under pure bending where the top bending stress is 171.4 MPa and also subjected to shear stress, the value of which is 17.1 MPa. Through a short calculation, it is possible to summarize different stress parameters useful for the design of the plate. Table 14 gives information about stress parameters whereas Table 15 gives the geometry of the steel plate.

In this example, only the plate element corresponding to the web girder has been modeled in Strand 7. The accurate mesh was done with Quad 4 plate elements of typical size equal to b/75 and each node was set to have six degrees of freedom. The first step of the design is to find the critical buckling load for the plate under patch loading F=300 kN.

From the numerical analysis, the critical buckling load multiplier was found to be equal to $\lambda_{\mathrm{cr},F}$=3.048 giving the critical buckling load equal to $F_{\mathrm{cr},F}^{\mathrm{FEM}} = 914.4$ kN. The information from Table 14 and Table 15 allows determination of the unknown coefficients c_1=0.790 and c_2=0.958 defined in Eqs. (22) and (23). Therefore, the analytical value of the critical buckling load $F_{\mathrm{cr},F}^{\mathrm{AN}} = 899.9$ kN is obtained throughout Eq. (21) and a good correlation between the two results is observed with only 1.5% standard deviation. The last step consists of finding both FEM and analytical results of the plate with interacting loads and comparing the two results. Through linear buckling analysis, to $\lambda_{\mathrm{cr},M+V+F}^{F}$ =1.602 the effect produced on critical patch loading resistance is observed as the new critical patch load will be $F_{\mathrm{cr},M+V+F}^{F,\mathrm{FEM}} = 480.6$ kN. The resistance has been quite reduced approximately to half. Before the calculation of the c_4 coefficient necessary for the use of

Table 13 Reduction coefficients c_4 taking into consideration interaction between patch loading, bending, and shear

ψ	Static scheme	c_4
−1.0	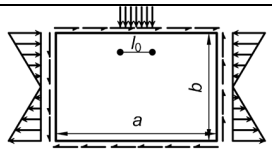	$\left(0.022\left(\frac{l_0}{a}\right)+0.023\right)\cdot A^2+\left(0.431\left(\frac{l_0}{a}\right)+0.260\right)\cdot B^2+\left(0.179\left(\frac{l_0}{a}\right)+0.163\right)\cdot A\cdot B$ $+\left(0.196\left(\frac{l_0}{a}\right)+0.107\right)\cdot A+\left(-0.329\left(\frac{l_0}{a}\right)-0.453\right)\cdot B+\left(-0.391\left(\frac{l_0}{a}\right)+1.145\right)$
−0.5	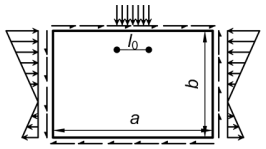	$\left(0.033\left(\frac{l_0}{a}\right)+0.029\right)\cdot A^2+\left(0.197\left(\frac{l_0}{a}\right)+0.332\right)\cdot B^2+\left(0.160\left(\frac{l_0}{a}\right)+0.244\right)\cdot A\cdot B$ $+\left(0.380\left(\frac{l_0}{a}\right)+0.112\right)\cdot A+\left(0.001\left(\frac{l_0}{a}\right)-0.673\right)\cdot B+\left(-0.593\left(\frac{l_0}{a}\right)+1.362\right)$
0.0	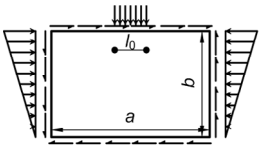	$\left(0.014\left(\frac{l_0}{a}\right)+0.043\right)\cdot A^2+\left(0.266\left(\frac{l_0}{a}\right)+0.320\right)\cdot B^2+\left(0.013\left(\frac{l_0}{a}\right)+0.289\right)\cdot A\cdot B$ $+\left(0.703\left(\frac{l_0}{a}\right)+0.050\right)\cdot A+\left(0.158\left(\frac{l_0}{a}\right)-0.721\right)\cdot B+\left(0.013\left(\frac{l_0}{a}\right)+0.289\right)$
1.0	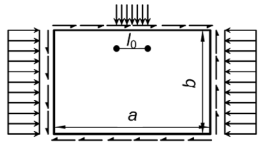	$\left(0.049\left(\frac{l_0}{a}\right)+0.037\right)\cdot A^2+\left(0.304\left(\frac{l_0}{a}\right)+0.317\right)\cdot B^2+\left(0.022\left(\frac{l_0}{a}\right)+0.300\right)\cdot A\cdot B$ $+\left(0.438\left(\frac{l_0}{a}\right)+0.067\right)\cdot A+\left(0.035\left(\frac{l_0}{a}\right)-0.705\right)\cdot B+\left(-0.603\left(\frac{l_0}{a}\right)+1.405\right)$

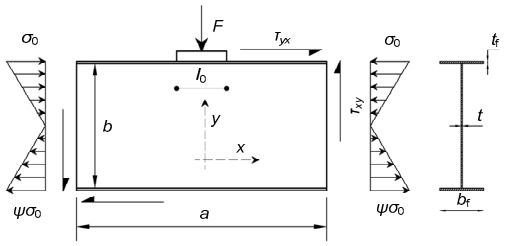

Fig. 14 Geometric and loading characteristic of the section studied

t_f: thickness of the steel flange; b_f: width of the steel flange

Table 14 Parametric data involved in the design formula

F (kN)	F_x (kN)	V_y (kN)	V_x (kN)	ψ	A	B	l_0/a
300	900	360	720	−1	3	0.4	0.2

Table 15 Geometrical characteristic of the steel section

a (mm)	t (mm)	b (mm)	t_f (mm)	b_f (mm)	λ	α
2200	14	1500	18	500	107.1	1.466

the analytical equation, A and B coefficients are provided. They are obtained through Eqs. (10) and (11) since they represent the relationship between patch loading, shear force, and bending moment. Therefore, from Eq. (24) with c_4 coefficient found in Table 13 considering the patch loading length corresponding to the design situation, the following result is obtained: c_4=1.602 and $F_{\mathrm{cr},M+V+F}^{F,\mathrm{AN}}=489.5$ kN. The difference between FEM and analytical results is less than 1.8%.

7 Conclusions

The stability of steel plates under combining patch loading, bending moment, and shear force was studied by means of numerical FEM analyses with Strand 7 software. In particular, extensive parametric analysis has been done to evaluate the effect of geometries and the combination of loads parameters. From the FEM analysis, it was determined that:

1. The slenderness is the most influential parameter of the plate stability;

2. The panel aspect ratio showed a slight influence with respect to the shear and bending actions;

3. The buckling deformation observed in the interaction of in-plane combined loadings depends on the amplitude of each load and is similar to either the buckling shape of steel plates under a single load or the combined deformation.

The influence of added bending and shear stress in a plate initially subjected to patch loading was investigated and an analytical formula was expressed to describe this influence.

The analytical formula provided a great accuracy since a comparison with the FEM analysis showed that for almost all cases, the deviation as inside the bounded region. Finally, a unique formula which

includes all four parameters is proposed because many engineers could use favorably this methodology to evaluate the critical buckling load. A design example has been added in order to prove the validity and good correlation was found between the analytical and FEM results. The conclusion from this example shows that the analytical formula is accurate for whatever plate geometry is used and it also showed that bending moment and shear stress can be reached due to the girder self-weight and construction loads may considerably reduce the critical buckling load.

References

Alinia MM, 2005. A study into optimization of stiffeners in plates subjected to shear loading. *Thin-Walled Structures*, 43(5):845-860. https://doi.org/10.1016/j.tws.2004.10.008

Alinia MM, Moosavi SH, 2009. Stability of longitudinally stiffened web plates under interactive shear and bending forces. *Thin-Walled Structures*, 47(1):53-60. https://doi.org/10.1016/j.tws.2008.05.005

Basler K, 1961. New Provisions for Plate Girder Design. American Institute of Steel Construction, p.65-74.

Braun B, 2010. Stability of Steel Plates under Combined Loading. PhD Thesis, Universität Stuttgart, Stuttgart, Germany.

CEN (European Committee for Standardization), 2006. Eurocode 3-Design of Steel Structures-part 1-5: Plated Structural Elements, EN 1993-1-5:2006. CEN.

Duchene Y, Maquoi R, 1994. Contribution, par voie numérique, à l'étude de la résistance des âmes aux charges transversales. *Construction Métallique*, 2:43-56 (in French).

Graciano C, Edlund B, 2003. Failure mechanism of slender girder webs with a longitudinal stiffener under patch loading. *Journal of Constructional Steel Research*, 59(1): 27-45. https://doi.org/10.1016/S0143-974X(02)00022-6

Graciano C, Lagerqvist O, 2003. Critical buckling of longitudinally stiffened webs subjected to compressive edge loads. *Journal of Constructional Steel Research*, 59(9): 1119-1146. https://doi.org/10.1016/S0143-974X(03)00055-5

Graciano C, Ayestarán A, 2013. Steel plate girder webs under combined patch loading, bending and shear. *Journal of Constructional Steel Research*, 80:202-212. https://doi.org/10.1016/j.jcsr.2012.09.018

Graciano C, Mendes J, 2014. Elastic buckling of longitudinally stiffened patch loaded plate girders using factorial design. *Journal of Constructional Steel Research*, 100:229-236. https://doi.org/10.1016/j.jcsr.2014.04.030

Graciano C, Zapata-Medina DG, 2015. Effect of longitudinal stiffening on bridge girder webs at incremental launching stage. *Ingeniería e Investigación*, 35(1):24-30. https://doi.org/10.15446/ing.investig.v35n1.42220

Jager B, Kövesdi B, Dunai L, 2017. I-girders with unstiffened slender webs subjected by bending and shear interaction. *Journal of Constructional Steel Research*, 131:176-188. https://doi.org/10.1016/j.jcsr.2017.01.009

Khan MZ, Walker AC, 1972. Buckling of plates subjected to localized edge loadings. *The Structural Engineer*, 50(6): 225-232.

Kövesdi B, Dunai L, 2016. Bending, shear and patch loading interaction behaviour of slender steel sections. *Procedia Engineering*, 156:199-206. https://doi.org/10.1016/j.proeng.2016.08.287

Kövesdi B, Alcaine J, Dunai L, et al., 2014. Interaction behaviour of steel I-girders part I: longitudinally unstiffened girders. *Journal of Constructional Steel Research*, 103: 327-343. https://doi.org/10.1016/j.jcsr.2014.06.018

Loaiza N, Graciano C, Chacón R, et al., 2017. Influence of bearing length on the patch loading resistance of multiple longitudinally stiffened webs. Proceedings of Eurosteel, 1(2-3):4199-4204.

Maiorana E, Pellegrino C, Modena C, 2008. Linear buckling analysis of unstiffened plates subjected to both patch load and bending moment. *Engineering Structures*, 30(12): 3731-3738. https://doi.org/10.1016/j.engstruct.2008.07.002

Maiorana E, Pellegrino C, Modena C, 2011. Influence of longitudinal stiffeners on elastic stability of girder webs. *Journal of Constructional Steel Research*, 67(1):51-64. https://doi.org/10.1016/j.jcsr.2010.07.005

Matlab, 2017. Matlab User's Manual, Version R2017a. MathWorks, Inc., USA.

Porter DM, Rockey KC, 1975. The collapse behaviors of plate girders loaded in shear. *Structural Engineering*, 53(8): 313-325.

Quang-Viet V, Papazafeiropoulos G, Graciano C, et al., 2019. Optimum linear buckling analysis of longitudinally multi-stiffened steel plates subjected to combined bending and shear. *Thin-Walled Structures*, 136:235-245. https://doi.org/10.1016/j.tws.2018.12.008

Ren T, Tong GS, 2005. Elastic buckling of web plates in I-girders under patch and wheel loading. *Engineering Structures*, 27(10):1528-1536. https://doi.org/10.1016/j.engstruct.2005.05.006

Rockey KC, Bagchi DK, 1970. Buckling of plate girder webs under partial edge loadings. *International Journal of Mechanical Sciences*, 12(1):61-76. https://doi.org/10.1016/0020-7403(70)90007-X

Shahabian F, Roberts TM, 1999. Buckling of slender web plates subjected to combinations of in-plane loading. *Journal of Constructional Steel Research*, 51(2):99-121. https://doi.org/10.1016/S0143-974X(99)00020-6

Strand 7, 2005. Strand 7 User's Manual. G+D Computing, Sydney, Australia.

Tetougueni CD, Maiorana E, Zampieri P, et al., 2019. Plate girders behaviour under in-plane loading: a review. *En-*

gineering Failure Analysis, 95:332-358. https://doi.org/10.1016/j.engfailanal.2018.09.021

Timoshenko S, Woinowsky-Krieger S, 1959. Theory of Plates and Shells. McGraw-Hill Book Company, New York, USA.

Tong GS, Feng YX, Tao WD, et al., 2016. Elastic stability of plate simply supported on four sides subjected to combined bending shear and patch loading. *Thin-Walled Structures*, 107:377-396. https://doi.org/10.1016/j.tws.2016.06.021

Zetlin L, 1955. Elastic instability of flat plates subjected to partial edge loads. *Proceedings of the American Society of Civil Engineers*, 81(9):1-24.

中文概要

题　目：钢结构梁中节点荷载、弯矩与剪应力的相互作用

目　的：通过深入的数值分析研究面内综合加载条件下钢板的临界屈曲荷载变化规律。

创新点：1. 提出一个确定钢梁在平面荷载作用下的临界屈曲系数的新公式；2. 通过与有限元分析结果对比以修正参数并获得解析公式的高精度。

方　法：1. 采用有限元分析软件 Strand 7 研究矩形钢板在节点荷载、弯矩和剪应力综合作用下的弹性稳定性；2. 针对节点荷载长度、载荷大小、板长宽比和长径比等参数分析对综合加载条件下的钢板稳定性的影响；3. 借助一个实际的例子验证解析公式的有效性。

结　论：1. 通过与有限元结果的比较，解析公式均表现出较高的精度，误差均在有限范围内且不受板几何形状的影响；2. 节点荷载、弯矩和剪应力的综合作用通过减小板临界抗屈曲性导致钢板的屈曲失效；3. 综合加载会导致临界抗屈曲性减小一半。

关键词：弹性稳定性；节点荷载；有限元分析；钢桥架设

Introducing Editorial Board Member:

Prof. Carlo PELLEGRINO has been the Editorial Board Member of *Journal of Zhejiang University-SCIENCE A (Applied Physics & Engineering)* since 2018. Carlo PELLEGRINO is a Full Professor of Structural Analysis and Design and Head of the Department of Civil, Environmental and Architectural Engineering, University of Padova, Italy. He is elected member of the Academic Senate, University of Padova, Italy. He obtained the PhD in Mechanics of Structures, University of Bologna, Italy. Prof. PELLEGRINO is coordinator of several national and international research projects, participant in COST Actions and referee for the selection of international research projects. He is member of various national and international technical and scientific associations.

He is author of over 300 scientific publications, over 100 of them in referred ISI/Scopus journals with more than 2500 citations (*h*-index 30) about the following topics: assessment, rehabilitation, strengthening and retrofit of buildings and bridges; seismic vulnerability and risk of existing buildings and bridges; integrated risk assessment and management of bridges in transportation networks; advanced strengthening techniques by means of innovative techniques; use of recycled components for structural materials.

He is a keynote speaker and member of the editorial board/international scientific committee of several international conferences and organizer of various special sessions/mini-symposia in international conferences. He is member of the organizing committee of various national and international conferences and Editorial Board Member of International Journals.